High Strength, Ductile Braze Repairs for Stationary Gas Turbine Components—Part II

Warren Miglietti

Madeleine Du Toit
Associate Professor

Department of Materials Science and Metallurgical Engineering,
University of Pretoria,
Pretoria 0002, South Africa

Both aviation and land based turbine components such as vanes/nozzles, combustion chambers, liners, and transition pieces often degrade and crack in service. Rather than replacing with new components, innovative repairs can help reduce overhaul and maintenance costs. These components are cast from either Co-based solid solution superalloys such as FSX-414, or Ni-based gamma prime precipitation strengthened superalloys such as IN738. The nominal compositions of FSX-414 and IN738 are Co–29.5Cr–10.5Ni–7W–2Fe (max)–0.25C–0.012B and Ni–0.001B–0.17C–8.5Co–16Cr–1.7Mo–3.4Al–2.6W–1.7Ta–2Nb–3.4Ti–0.1Zr, respectively. Diffusion brazing has been used for over 4 decades to repair cracks and degradation on these types of components. Typically, braze materials utilized for component repairs are Ni and Co-based braze fillers containing B and/or Si as melting point depressants. Especially when repairing wide cracks typically found on industrial gas turbine components, these melting point depressants can form brittle intermetallic boride and silicide phases that effect mechanical properties such as low cycle and thermal fatigue. The objective of this work is to investigate and evaluate the use of hypereutectic Ni–Cr–Hf and Ni–Cr–Zr braze filler metals, where the melting point depressant is no longer B, but Hf and/or Zr. Typically, with joint gaps or crack widths less than 0.15 mm, the braze filler metal alone can be utilized. For cracks greater than 0.15 mm, a superalloy powder is mixed with the braze filler metal to enable wide cracks to be successfully braze repaired. As a means of qualifying the diffusion braze repair, both metallurgical and mechanical property evaluations were carried out. The metallurgical evaluation consisted of optical and scanning electron microscopy, and microprobe analysis. The diffusion brazed area consisted of a fine-grained equiaxed structure, with carbide phases, γ (gamma) dendrites, flower shaped/rosette γ-γ' (gamma-gamma prime) eutectic phases and Ni_7Hf_2, Ni_5HF, or Ni_5Zr intermetallic phases dispersed both intergranularly and intragranularly. Hardness tests showed that the Ni–Hf and Ni–Zr intermetallic phase only has a hardness range of 250–400 Hv; whereas, the typical Cr-boride phases have hardness ranges from 800 Hv to 1000 Hv. Therefore, the hardness values of the Ni–Hf and Ni–Zr intermetallic phases are 2.5–3.2 times softer than the Cr-boride intermetallic phases. As a result, the low cycle fatigue (LCF) properties of the wide gap Ni–Cr–Hf and Ni–Cr–Zr brazed joints are superior to those of the Ni–Cr–B braze filler metals. The mechanical property evaluations were tensile tests at both room temperature and elevated temperature, stress rupture tests from 760°C to 1093°C and finally LCF, the latter being one of the most important and severe tests to conduct, since the cracks being repaired are thermal fatigue driven. At the optimum braze thermal cycle, the mechanical test results achieved were a minimum of 80% and sometimes equivalent to that of the base metals properties. [DOI: 10.1115/1.4000149]

1 Introduction

Over the last two decades numerous technical papers have been published on narrow gap (0.025 mm—0.127 mm) and wide gap (greater than 0.127 mm) brazing for the manufacture [1–10] and repair [11–27] of nickel and cobalt-based gas turbine engine components. In all these technical papers, boron (B) and/or silicon (Si) were utilized as melt point depressants, except with Laux et al. [27] where manganese (Mn) was utilized as a melt point depressant.

Examination of the binary phase diagrams with nickel as solvent revealed that hafnium (Hf) and zirconium (Zr) might be suitable for use as melting point depressants in novel braze filler metals for repairing Ni-based superalloy components. Nash and Nash [21] reported the existence of an invariant eutectic reaction in the Ni–Hf binary system at a composition of 30.5 wt % Hf and 69.5 wt % Ni (see Fig. 1 below). The eutectic temperature was quoted as 1190°C. Similarly, Nash and Jayanth [22] reported that the Ni–Zr binary system also contains a eutectic point located at 13 wt % Zr and 87 wt % Ni (see Fig. 2 below). The eutectic temperature was quoted as 1170°C. In order to determine whether Hf and Zr can be used as melting point depressants in Ni-based braze filler metals, Ni and Cr powders were mixed with Hf or Zr powder to make up simple tertiary braze compositions.

Upon determining that a Ni–Cr–Hf or Ni–Cr–Zr braze can indeed be utilized to join two Ni-based superalloys together, these braze alloys were mixed with a superalloy powder to determine if wide gap brazed joints can be produced.

The objectives of this research work are as follows:

- Demonstrate that the two hypereutectic braze alloys consisting of Ni–Cr–Hf and Ni–Cr–Zr, can successfully melt and flow like typical braze alloys used in the aerospace industry or industrial gas turbine (IGT) industry.

Contributed by the International Gas Turbine Institute of ASME for publication in the JOURNAL OF ENGINEERING FOR GAS TURBINES AND POWER. Manuscript received May 7, 2009; final manuscript received May 7, 2009; published online May 11, 2010. Editor: Dilip R. Ballal.

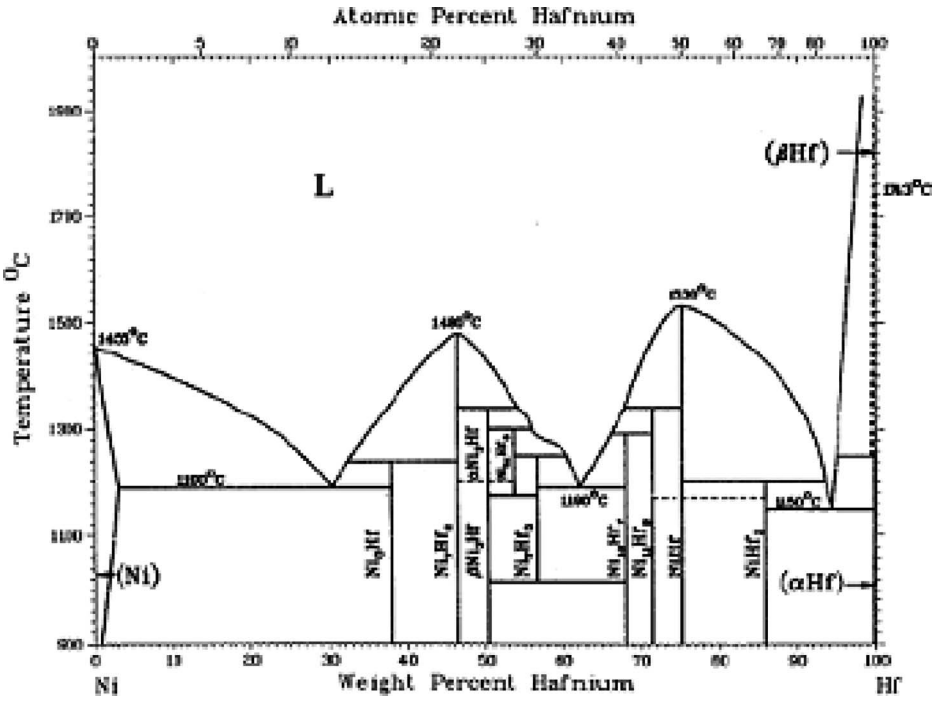

Fig. 1 Binary Ni–Hf phase diagram [21]

- Determine the microstructure of the two braze joints and quantitatively and qualitatively analyze the resultant intermetallic phases formed in the joint. Optical, scanning electron microscopy (SEM), and electron microprobe (EPMA) results will be documented in this paper.
- Demonstrate that the two braze alloys consisting of Ni–Cr–Hf and Ni–Cr–Zr, can successfully be used in combination with a Ni-based superalloy powder MarM247 (Ni–0.001B–0.15C–10Co–8.25Cr–1.5Hf–0.7Mo–5.5Al–10W-3Ta–1Ti–0.05Zr–0.5Fe) as part of the wide gap diffusion brazing process.
- Evaluate the tensile, stress rupture, and low cycle fatigue properties of the wide gap braze joints. Some of the tensile and stress rupture properties were already published in the Part I paper, i.e., GT2000-51133, published at the ASME Turbo Expo conference in June 2008, in Berlin, Germany.

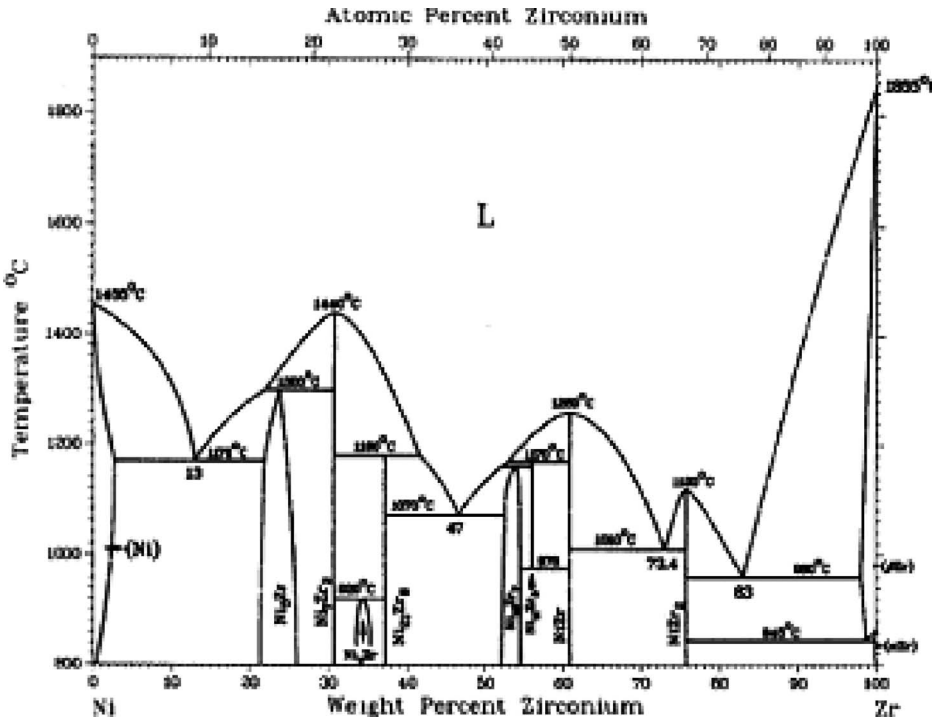

Fig. 2 Binary Ni–Zr phase diagram [22]

2 Experimental Procedure

2.1 Metallurgical Evaluation. IN738 flat plates of composition Ni–0.001B–0.17C–8.5Co–16Cr–1.7Mo–3.4Al–2.6W–1.7Ta–2Nb–3.4Ti–0.1Zr were excised from the roots of scrap blades by electrical discharge machining (EDM). The root of a blade is not exposed to any appreciable temperature and stress in service; hence, material taken from this area is normally referred to as virginlike as-cast material. After the EDM process, the material was ground down in a surface grinder to 2 mm thickness with various lengths and widths. These plates were subsequently cleaned by grit blasting with 220 grit silicon carbide media. The plates were then wiped with acetone to remove the residue left over from grit blasting. The hypereutectic Ni–Cr–Hf and/or Ni–Cr–Zr braze alloy, together with the MarM247 powder, were mixed with a binder to form a paste. After the acetone evaporated, either the Ni–Cr–Hf/MarM247 or Ni–Cr–Zr/MarM247 paste was applied between two plates (like a filling in a sandwich, i.e., a 1.5 mm butt joint). The samples, one group where the Ni–Cr–Hf braze alloy was used, and the other samples where the Ni–Cr–Zr braze alloy was used, were allowed to dry in air for 1 h before vacuum heat treating in a laboratory furnace with a maximum temperature capability of 1300°C. Because the furnace does not have quench capability, the samples were slow cooled (furnace cooled) to room temperature.

The vacuum cycle used was as follows:

(1) Ramp up at a rate of 15°F/min minimum, to a temperature of 450°C.
(2) Hold at 450°C for 20 min to let the binder burn off/burn away.
(3) Ramp up at a rate of 15°F/minute minimum, to a temperature of 1150°C.
(4) Hold at 1150°C for 20 min to let the samples stabilize at this temperature.
(5) Ramp up at a rate of 15°F/min minimum, to a temperature of 1238°C, to get the braze alloy to melt and flow. Note: a proprietary homogenization heat treatment was given to the IN738 material prior to brazing to prevent incipient melting during the braze thermal cycle.
(6) Hold at the temperatures in (5) above for times varying from 40 min to 24 h.
(7) Furnace cool to room temperature.

After exposing the samples to a vacuum braze cycle as mentioned above, the samples were sectioned and mounted using conventional metallographic practices. The metallographic mounts were etched with Marbles reagent to reveal the microstructure. Optical and SEM microscopy were performed. The optical microscope was a Nikon Epiphot 200 model, with a maximum magnification capability of 1000×. The SEM instrument was a JOEL-Oxford model, using the ZAF software correction. The acceleration voltage was 20 kV, the % dead time was approximately 50 s, the sample tilt angle was 0 deg, and the acquisition time was 150 s.

For the microprobe analysis the brazed samples were mounted in resin and prepared using conventional metallographic techniques. The mounted samples were carbon coated using a sputtering technique and electrically grounded with copper tape to minimize charging of the specimens by the microprobe electron beam. Calibration was performed using polished pure element standards.

Analysis conditions were established for either a 15 keV or 20 keV focused electron beam, adjusted to provide 35 nA of specimen current on pure nickel. Desired locations for analysis were selected by generating a backscatter electron (BSE) image before placing the instrument in "spot mode," during which the focused beam was directed to selected locations within the area shown in the BSE image. The BSE images were annotated to highlight the features subjected to elemental characterization by energy dispersive X-ray spectroscopy (EDS). The EDS peak identifications were verified using a wavelength dispersive X-ray spectrometer (WDS), tuned to the elements of interest. X-ray intensity data were collected in triplicate at each selected location. Measured X-ray counts were then converted to elemental weight percentages using commercially available algorithms.

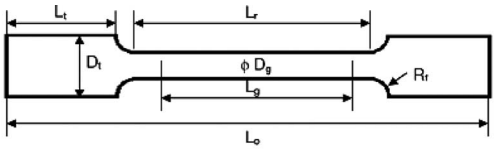

D_{gauge}=4.57mm, L_{gauge}=18.29mm, L_r=21.84mm, R_r =3.18mm, $L_{overall}$=46.51mm, D_t=7.94mm [5/16-24NF-2A inches] and L_t=9.53mm

Fig. 3 Configuration of tensile and stress rupture test specimens

3 Tensile, Stress Rupture, and Low Cycle Fatigue Testing

Tensile tests results on MarM247 base metal at 22°C and elevated temperatures of 650°C, 760°C, 870°C, and 980°C, as well some stress rupture test results on IN738 base metal were already discussed for brazed joints held at temp for a max time of 4 h, in the Part I paper, i.e., GT2000-51133, published at the ASME Turbo Expo conference in June 2008 in Berlin, Germany. The tensile test configuration can be found in Fig. 3, where the braze is in a 1.5 mm butt joint configuration.

Stress rupture tests were conducted as shown in Table 1. IN738 specimens were joined together at 1238°C for 12 h, followed by a solution heat treatment (SHT) or hot isostatic pressure (HIP) cycle. The stress rupture test specimens were also prepared in a butt joint configuration as seen in Fig. 3, where the joint gap is 1.5 mm.

For LCF testing, investment cast plates of IN738 material of dimensions: 9.75 in. long, 5 in. wide, and 0.600 in. thick were obtained, as seen in Fig. 4. A 1.5 mm groove was machined along the length, in the middle of the plate, as seen in Fig. 5, to simulate the typical larger crack width found in IGT stationary nozzles, as opposed to generally smaller crack widths typically found in aircraft gas turbine nozzles/vanes.

After machining, the groove was cleaned by grit blasting with 220 grit silicon carbide media. After all braze and thermal processing, 12.7 mm diameter low cycle fatigue test specimens were machined from the plates in such a way that each braze joint formed a full butt joint in the center of the gauge length. The ends of the samples were threaded and the diameter of the gauge length

Table 1 Stress rupture test conditions

Temperature (°C)	Stress level (MPa)	Stress level (MPa)	Stress level (MPa)
900	242	186	152
845	345		
980	138		

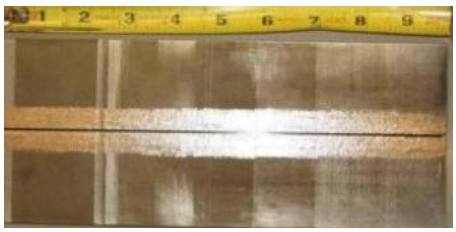

Fig. 4 Plate of 247.7 mm length with 1.5 mm groove machined in the center

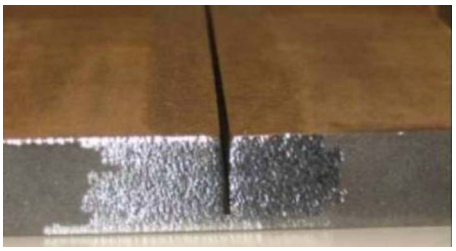

Fig. 5 1.5 mm groove machined down the center/middle of the plate

reduced to 6.35 mm as seen in Fig. 6. The 1.5 mm wide gap braze joint is in the center of the gauge length, to simulate a typical crack width found in an IGT engine operated nozzle segment, as seen in Fig. 7.

Low cycle fatigue tests on IN738 base metal were performed at a test temperature of 870°C under strain control conditions. The tests were performed at a constant strain rate of 0.01 s^{-1} with a symmetrical triangular waveform. The total strain was varied from 0.3% to 2% and the test frequency from 1 Hz to 0.33 Hz. A constant A-ratio (defined below) of +1 was maintained during testing.

$$\text{A-ratio} = (\text{maximum strain} - \text{minimum strain})/(\text{maximum strain} + \text{minimum strain})$$

4 Metallurgical and Mechanical Test Results

4.1 Metallurgical Results and Discussion

4.1.1 Hypereutectic Ni–Cr–Hf Brazed Joints—Optical Microscopy. Figure 8 shows the microstructure of a wide gap brazed joint, where MarM247 superalloy powder was mixed with the Ni–Cr–Hf braze filler metal and processed at 1238°C for 4 h. The joint is composed of a majority of the prior superalloy powder particles, eutectic and Ni_7Hf_2 intermetallic phases, and a thin layer of γ dendrites/phases that are bonding/sintering the Ni-based superalloy powder particles together.

Figure 9 shows the microstructure of a wide gap brazed joint produced at 1238°C for 12 h, followed by a 1232°C for 4 h SHT. Percentage wise, the joint is composed of a majority of the MarM247 powder particles, eutectic phases (γ phase+Ni_7Hf_2 phase), plus solid Ni_7Hf_2 intermetallic phases that are left at the grain boundaries.

Fig. 6 Configuration of tensile and stress rupture test specimens

Fig. 7 1.5 mm wide cracks on the sidewalls of a typically industrial gas turbine nozzle segment

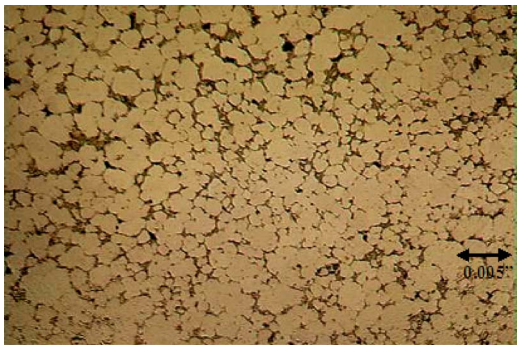

Fig. 8 Microstructure of MarM247 superalloy powder mixed with the Ni–Cr–Hf braze, produced at 1238°C for 4 h

Figure 10 shows the microstructure of a wide gap brazed joint produced at 1238°C for 12 h, followed by a 1232°C for 4 h SHT, followed by a 1080°C for 4 h HIP cycle at 25ksi pressure. The joint is composed of a majority of the MarM247 powder particles sintered together, with intergranular eutectic phases (γ phase +Ni_7Hf_2 phase), plus solid Ni_7Hf_2 intermetallic phases.

4.1.2 Hypereutectic Ni–Cr–Zr Brazed Joints—Optical Microscopy. Figure 11 shows that microstructure of a wide gap brazed joint, produced at 1238°C for 4 h, where MarM247 powder was mixed with the Ni–Cr–Zr braze filler metal. The joint is composed of a majority of the prior superalloy powder particles,

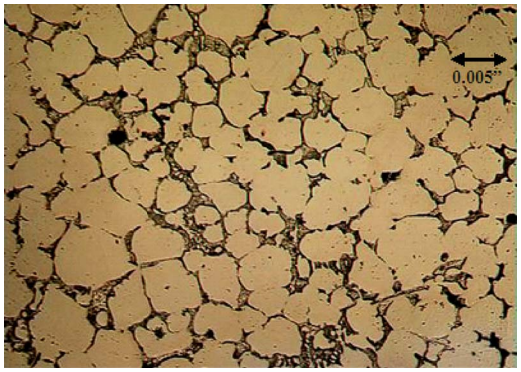

Fig. 9 Microstructure of MarM247 superalloy powder mixed with the Ni–Cr–Hf braze, produced at 1238°C for 12 h +1232°C for 4 h (SHT)

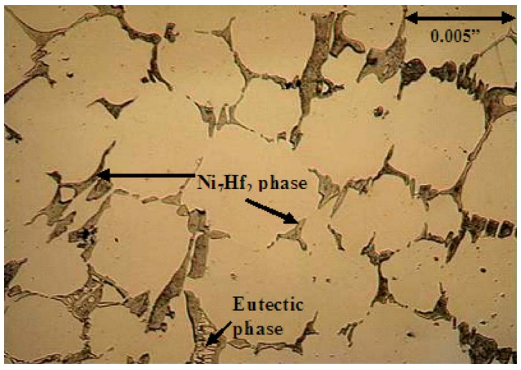

Fig. 10 Microstructure of MarM247 superalloy powder mixed with the Ni–Cr–Hf braze, produced at 1238°C for 12 h +1232°C for 4hrs SHT and a HIP cycle at 1080°C for 4 h

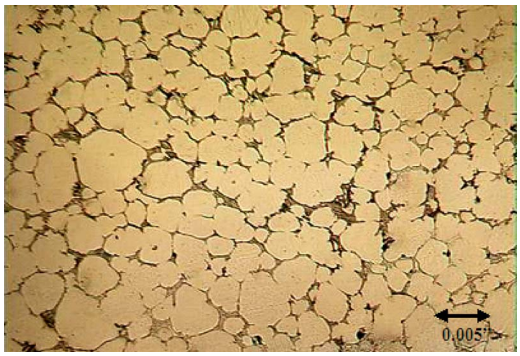

Fig. 11 Microstructure of MarM247 superalloy powder mixed with the Ni–Cr–Zr braze, produced at 1238°C for 4 h

eutectic and Ni_5Zr intermetallic phases, and a thin layer of γ dendrites/phases and that are bonding/sintering the superalloy powder particles together.

Figure 12 shows the microstructure of a wide gap brazed joint produced at 1238°C for 12 h, followed by a 1232°C for 4 h SHT. Percentage wise, the joint is composed of a majority of the MarM247 powder particles, eutectic phases (γ phase+Ni_5Zr phase), plus solid Ni_5Zr intermetallic phases that are left at the grain boundaries.

Figure 13 shows the microstructure of a wide gap brazed joint produced at 1238°C for 12 h, followed by a 1232°C for 4 h SHT, followed by a 1080°C for 4 h at 25 ksi pressure HIP cycle. The joint is composed of a majority of the MarM247 powder particles

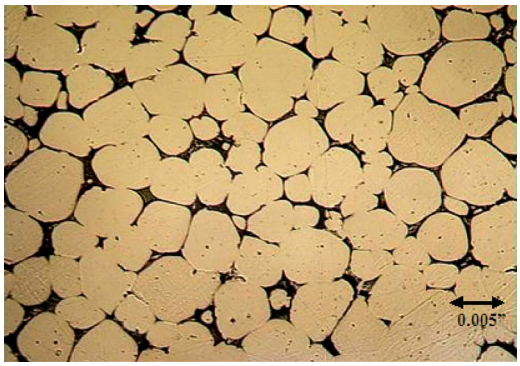

Fig. 12 Microstructure of MarM247 superalloy powder mixed with the Ni–Cr–Zr braze, produced at 1238°C/12 h +1232°C/4 h (SHT)

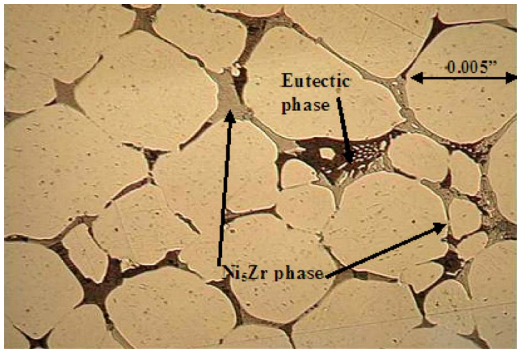

Fig. 13 Microstructure of MarM247 superalloy powder mixed with the Ni–Cr–Zr braze, produced at 1238°C/12 h +1232°C/4 h (SHT) and a HIP cycle at 1080°C for 4 h

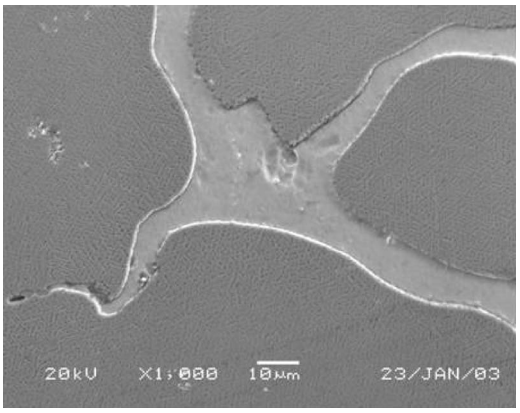

Fig. 14 SEM micrograph of the Ni–Cr–Hf braze, showing the intergranular Ni_7Hf_2 intermetallic phase

sintered together, with intergranular eutectic phases (γ phase +Ni_5Zr phase), plus solid Ni_5Zr intermetallic phases.

4.1.3 Hypereutectic Ni–Cr–Hf Brazed Joints—SEM Evaluation. The intermetallic phases were analyzed in the wide gap brazed joint shown in Fig. 14, where the MarM247 superalloy powder was mixed with the Ni–Cr–Hf braze filler metal, and processed at 1230°C for 12 h, followed by solution annealing and HIP'ing. The energy dispersive X-ray analysis revealed a composition of 52.21Ni–44.72Hf–2.11Co–0.53Cr–0.17Ti–0.26W (wt %), and was provisionally identified as the Ni_7Hf_2 intermetallic compound. Nash and Nash [21] reported that the Ni_7Hf_2 intermetallic phase contains 46.5% Hf; whereas, the Ni_5Hf phase contains 37.9% Hf. Therefore it appears that the Ni_7Hf_2 intermetallic phase that existed here contains essentially Ni and Hf, but Co, Cr, W, and Ti are soluble in this phase to a small extent.

Figure 15 shows that a fine, cuboidal gamma prime (γ') phase had precipitated within the MarM247 γ matrix. The cuboidal and spheroidal γ' precipitates in MarM247 generally form during primary and secondary aging cycles at 1080°C for 4 h, followed by soaking at 870°C for 24 h. The HIP cycle used in this investigation therefore overlapped with the primary aging treatment for MarM247, resulting in some γ' precipitation within the γ phase.

4.1.4 Hypereutectic Ni–Cr–Zr Brazed Joints—SEM Evaluation. The intermetallic phases were analyzed in the wide gap brazed joint shown in Fig. 16, where the MarM247 superalloy powder was mixed with the Ni–Cr–Zr braze filler metal, and processed at 1230°C for 12 h, followed by solution annealing and HIP'ing. The energy dispersive X-ray analysis revealed a

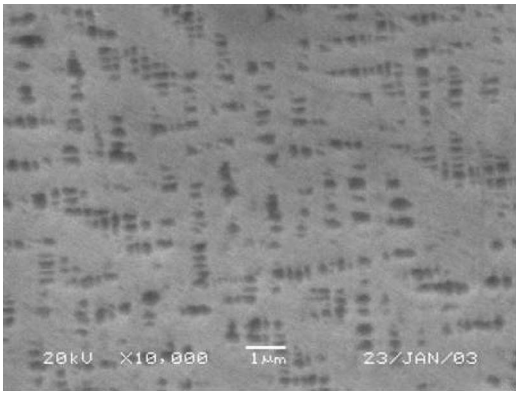

Fig. 15 SEM micrograph of the Ni–Cr–Hf braze, showing cuboidal γ' precipitates within the MarM247 powder particles

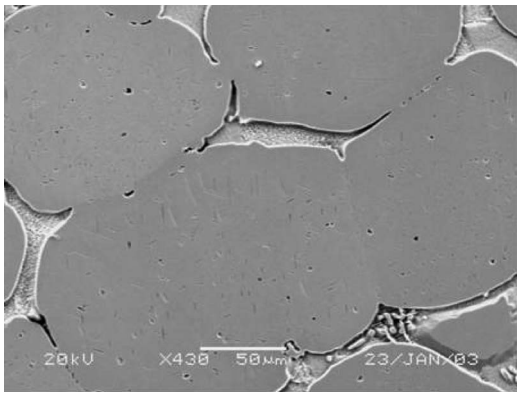

Fig. 16 SEM micrograph of the Ni–Cr–Hf braze, showing the intergranular Ni_5Zr intermetallic phase

composition of 72.18Ni–24.43Zr–2.18Co–0.64Cr–0.45Al–0.28W (wt %), and was provisionally identified as Ni_5Zr. As was the case shown in Fig. 15, there was also some γ' precipitation within the γ phase.

4.1.5 Hypereutectic Ni–Cr–Hf Brazed Joints—EPMA Evaluation. In order to perform a more detailed analysis of the intermetallic phases observed in the braze joint, since the EDS results are at best semiquantitative, three spot chemical analyses were performed within the intermetallic phases in the braze joint, using EPMA. A backscattered electron image of the MarM247/Ni–Cr–Hf braze joint shown in Fig. 17, has the location of the three phases analyzed highlighted. The results of the microprobe phase analyses indicate the following:

- Phase 1: Ni–31.53Hf–8.43Zr–3.55Ta–3.37Co–0.84Cr–0.29Al–0.15Mo–0.07W
- Phase 2: Ni–31.09Hf–8.54Zr–3.59Ta–3.1Co–0.71Cr–0.29Al–0.18Mo–0.08W
- Phase 3: Ni–36.34Hf–5.30Zr–3.91Ta–3.63Co–0.62Cr–0.29 Al–0.15Mo–0.13W

The results suggest that the intermetallic phase within the braze alloy contained between 31% and 36% Hf (wt %). The binary Ni–Hf phase diagram, shown in Fig. 1, indicates that the Ni_5Hf intermetallic phase contains approximately 38 wt% Hf, whereas the Ni_7Hf_2 intermetallic phase contains about 46 wt % Hf. The results found during the EPMA evaluation therefore suggest that

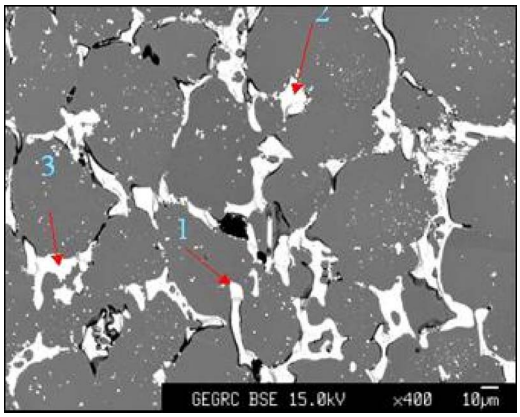

Fig. 17 Secondary electron image of the Ni–Cr–Hf braze, highlighting the location of three spot chemical analyses of the intermetallic phases within the braze

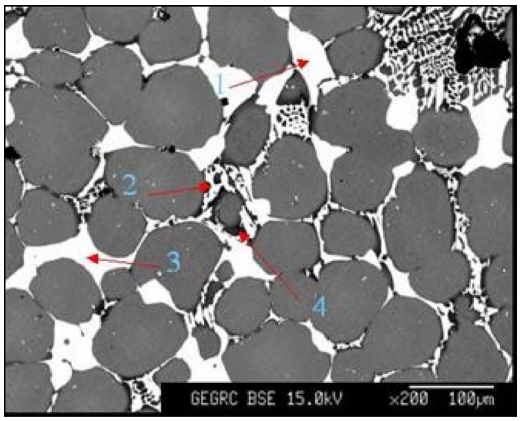

Fig. 18 Secondary electron image of the Ni–Cr–Zr braze, highlighting the location of four spot chemical analyses of the intermetallic phases within the braze

the intermetallic phase in the braze joint is Ni_5Hf, rather than Ni_7Hf_2.

It is, however, interesting to note that the Hf-rich phase identified here contained high levels of Zr (between 7.4% and 9.6%), probably present as a contaminant in the Ni–Cr–Hf powder as well as diffusion from the MarM247 powder that segregated preferentially to the intermetallic phase on solidification, and approximately 3% Ta, which may be present as a result of dilution with the MarM247 powder particles during brazing. The presence of Zr and Ta may shift the composition of the Hf-rich intermetallic phase away from the equilibrium composition predicted by the phase diagram. If it is assumed that the intermetallic phase contained between 7.4% and 9.6% Zr in solution, as well as 3% Ta, its composition may well approach that of the Ni_7Hf_2 (or rather $Ni_7(Hf,Zr,Ta)_2$) intermetallic compound.

4.1.6 Hypereutectic Ni–Cr–Zr Brazed Joints—EPMA Evaluation. In order to perform a more detailed analysis of the intermetallic phases observed in the braze joint, since the EDS results are at best semiquantitative, three spot chemical analyses were performed within the intermetallic phases in the braze joint, using EPMA. A backscattered electron image of the MarM247/Ni–Cr–Zr braze joint is in Fig. 18, has the location of the four phases analyzed highlighted. The results of the microprobe phase analyses indicate the following:

- Phase 1: Ni–26.87Zr–1.6Hf–1.83Co–1.39Ta–0.6Cr–0.35W–0.05Mo–0.18Al–0.08Ti
- Phase 2: Ni–26.97Zr–1.43Hf–1.81Co–1.33Ta–0.77Cr–0.07W–0.07Mo–0.19Al–0.14Ti
- Phase 3: Ni–26.65Zr–1.71Hf–1.85Co–1.81Ta–0.61Cr–0.45W–0.09Mo–0.17Al–0.10Ti
- Phase 4: Ni–0.63Zr–0.04Hf–4.53Co–1.58Ta–9.13Cr–3.35 W–0.42Mo–3.16Al–0.55Ti

The results suggest that the intermetallic phase within the braze alloy (phases 1, 2, and 3) contained between 26% and 27% Zr, as well as some Hf, Ta, and Co. Phase 4, was most likely the Ni-rich γ phase, with some Cr, Co, and W in solution. The binary Ni–Zr phase diagram, shown in Fig. 2, indicates that the Ni_7Zr_2 intermetallic phase contains approximately 30 wt % Zr, whereas the Ni_5Zr intermetallic compound contains approximately between 21 wt % and 26 wt % Zr. The results shown above therefore suggest that the intermetallic phase in the braze joint would be rather Ni_5Zr in lieu of the Ni_7Zr_2 compound.

Table 2 Tensile results at 22°C of the brazed specimens

Tensile properties	Ni–Cr–Hf joints 1230°C for 4 h	Ni–Cr–Zr joints 1230°C for 4 h	Ni–Cr–Hf joints 1230°C for 12 h+SHT+HIP	Ni–Cr–Zr joints 1230°C for 12 h+SHT+HIP	Mar-M247 base metal
UTS (MPa)	344	564	713	736	960
YS (MPa)	302	511	644	662	800
RA (%)	3.9	4.5	5.6	8.0	10.0

5 Mechanical Properties—Results and Discussion

5.1 Tensile Test Results and Discussion. Tables 2–5 show the tensile test results of the wide gap brazed joints at various temperatures. All test results are an average of three specimens. UTS=ultimate tensile strength, YS=yield strength, and RA =reduction in area. It should be noted that since cylindrical samples, as opposed to flat plate tensile samples, were utilized during tensile testing, the RA value is a more realistic representation of the ductility of the braze joint in lieu of the elongation value. Hence, any reference to braze ductility is characterized mainly by the RA value in lieu of the elongation value.

As seen in Table 2, at room temperature, the tensile and yield strengths of the Ni–Cr–Hf joints, produced at 1238°C/12 h, followed by a 1232°C/4 h SHT, and then followed by a 1080°C/4 h HIP, are 74.3% and 80.4%, respectively, of the MarM247 base metals properties. In contrast, the tensile and yield strengths of the Ni–Cr–Hf joints, produced at 1238°C/4 h, are 36% and 38%, respectively, of the base metals properties. This clearly shows that as the time at temperature is increased for the Ni–Cr–Hf joints, the tensile and yield strengths increased. Similarly as seen in Table 2, the tensile and yield strengths of the Ni–Cr–Zr joints produced at 1238°C/12 h, followed by a 1232°C/4 h SHT, and then followed by a 1080°C/4 h HIP, are 76.8% and 77.7%, respectively, of the MarM247 base metals properties. In contrast, the tensile and yield strengths of the Ni–Cr–Zr joints, produced at 1238°C/4 h, are 59% and 64%, respectively, of the MarM247 base metals properties. This clearly shows that as the time of the temperature is increased for the Ni–Cr–Zr joints, the tensile and yield strengths increased. Also as seen in Table 2, the ductility of the Ni–Cr–Hf joints, produced at 1238°C/12 h, followed by a 1232°C/4 h SHT, and then followed by a 1080°C/4 h HIP, are 56% of the MarM247 base metals ductility. In contrast, the ductility of the Ni–Cr–Hf joints, produced at 1238°C/4 h, are 39% of the base metals ductility. This clearly showed that as the time at temperature is increased for the Ni–Cr–Hf joints, the ductility also increased. Similarly as seen in Table 2, the ductility of the Ni–Cr–Zr joints, produced at 1238°C/12 h, followed by a 1232°C/4 h SHT, and then followed by a 1080°C/4 h HIP, are 80% of the MarM247 base metals ductility. In contrast, the ductility of the Ni–Cr–Zr joints, produced at 1238°C/4 h, are 45% of the base metals ductility. This clearly showed that as the time of temperature is increased for the Ni–Cr–Zr joints, the ductility also increased.

As seen in Table 3, at 540°C, the tensile and yield strengths of the Ni–Cr–Hf joints, produced at 1238°C/12 h, followed by a 1232°C/4 h SHT, followed by a 1080°C/4 h HIP, are 73% and 81%, respectively, of the MarM247 base metals properties. In contrast, the tensile and yield strengths of the Ni–Cr–Hf joints, produced at 1238°C/4 h, are 40% and 41%, respectively, of the base metals properties. This clearly shows that as the time of temperature is increased for the Ni–Cr–Hf joints, the tensile and yield strengths increased. Similarly, as seen in Table 3, the tensile and yield strengths of the Ni–Cr–Zr joints produced at 1238°C/12 h, followed by a 1232°C/4 h SHT, and then followed by a 1080°C/4 h HIP, are 98% and 88%, respectively, of the MarM247

Table 3 Tensile results at 540°C of the brazed specimens

Tensile properties	Ni–Cr–Hf joints 1230°C for 4 h	Ni–Cr–Zr joints 1230°C for 4 h	Ni–Cr–Hf joints 1230°C for 12 h+SHT+HIP	Ni–Cr–Zr joints 1230°C for 12 h+SHT+HIP	Mar-M247 base metal
UTS (MPa)	406	625	740	999	1014
YS (MPa)	329	556	647	707	801
RA (%)	3.8	3.4	5.3	7.9	9.9

Table 4 Tensile results at 870°C of the brazed specimens

Tensile properties	Ni–Cr–Hf joints 1230°C for 4 h	Ni–Cr–Zr joints 1230°C for 4 h	Ni–Cr–Hf joints 1230°C for 12 h+SHT+HIP	Ni–Cr–Zr joints 1230°C for 12 h+SHT+HIP	Mar-M247 base metal
UTS (MPa)	342	480	544	743	790
YS (MPa)	277	404	458	650	650
RA (%)	3.2	3.1	4.2	6.0	7.7

Table 5 Tensile results at 980°C of the brazed specimens

Tensile properties	Ni–Cr–Hf joints 1230°C for 4 h	Ni–Cr–Zr joints 1230°C for 4 h	Ni–Cr–Hf joints 1230°C for 12 h+SHT+HIP	Ni–Cr–Zr joints 1230°C for 12 h+SHT+HIP	Mar-M247 base metal
UTS (MPa)	266	308	282	311	506
YS (MPa)	206	214	223	239	312
RA (%)	3.1	6.2	5.7	6.9	7.5

base metals properties. In contrast, the tensile and yield strengths of the Ni–Cr–Zr joints, produced at 1238°C/4 h, are 62% and 70%, respectively, of the MarM247 base metals properties. This clearly shows that as the time at temperature is increased for the Ni–Cr–Zr joints, the tensile and yield strengths increased. Also as seen in Table 3, the ductility of the Ni–Cr–Hf joints, produced at 1238°C/12 h, followed by a 1232°C/4 h SHT, and then followed by a 1080°C/4 h HIP, are 54% of the MarM247 base metals ductility. In contrast, the ductility of the Ni–Cr–Hf joints, produced at 1238°C/4 h, are 39% of the base metals ductility. This clearly showed that as the time at temperature is increased for the Ni–Cr–Hf joints, the ductility also increased. Similarly as seen in Table 3, the ductility of the Ni–Cr–Zr joints, produced at 1238°C/12 h, followed by a 1232°C/4 h SHT, and then followed by a 1080°C/4 h HIP, are 80% of the MarM247 base metals ductility. In contrast, the ductility of the Ni–Cr–Zr joints, produced at 1238°C/4 h, are 35% of the base metals ductility. This clearly showed that as the time at temperature is increased for the Ni–Cr–Zr joints, the ductility levels increased.

As seen in Table 4, at 870°C, the tensile and yield strengths of the Ni–Cr–Hf joints, produced at 1238°C/12 h, followed by a 1232°C/4 h SHT, and then followed by a 1080°C/4 h HIP, are 69% and 71%, respectively, of the MarM247 base metals properties. In contrast, the tensile and yield strengths of the Ni–Cr–Hf joints, produced at 1238°C/4 h, are 43% and 43%, respectively, of the base metals properties. This clearly shows that as the time at temperature is increased for the Ni–Cr–Hf joints, the tensile and yield strengths increased. Similarly as seen in Table 4, the tensile and yield strengths of the Ni–Cr–Zr joints, produced at 1238°C/12 h, followed by a 1232°C/4 h SHT, followed by a 1080°C/4 h HIP, are 94% and 100%, respectively, of the MarM247 base metals properties. In contrast, the tensile and yield strengths of the Ni–Cr–Zr joints, produced at 1238°C/4 h, are 61% and 62%, respectively, of the MarM247 base metals properties. This clearly shows that as the time at temperature is increased for the Ni–Cr–Zr joints, the tensile and yield strengths increased. Also as seen in Table 4, the ductility of the Ni–Cr–Hf joints, produced at 1238°C/12 h, followed by a 1232°C/4 h SHT, and then followed by a 1080°C/4 h HIP, are 55% of the MarM247 base metals ductility. In contrast, the ductility of the Ni–Cr–Hf joints, produced at 1238°C/4 h, are 42% of the base metals ductility. This clearly showed that as the time at temperature is increased for the Ni–Cr–Hf joints, so too did the ductility. Similarly as seen in Table 4, the ductility of the Ni–Cr–Zr joints, produced at 1238°C/12 h, followed by a 1232°C/4 h SHT, followed by a 1080°C/4 h HIP, are 78% of the MarM247 base metals ductility. In contrast, the ductility of the Ni–Cr–Zr joints, produced at 1238°C/4 h, are 40% of the base metals ductility. This clearly showed that as the time at temperature is increased for the Ni–Cr–Zr joints, the ductility levels increased.

Finally, as seen in Table 5, at 980°C, the tensile and yield strengths of the Ni–Cr–Hf joints, produced at 1238°C/12 h, followed by a 1232°C/4 h SHT, followed by a 1080°C/4 h HIP, are 56% and 72%, respectively of the MarM247 base metals properties. In contrast, the tensile and yield strengths of the Ni–Cr–Hf joints, produced at 1238°C/4 h, are 53% and 66%, respectively, of the base metals properties. This clearly shows that as the time of temperature is increased for the Ni–Cr–Hf joints, the tensile and yield strengths increased. Similarly as seen in Table 5, the tensile and yield strengths of the Ni–Cr–Zr joints, produced at 1238°C/12 h, followed by a 1232°C/4 h SHT, followed by a 1080°C/4 h HIP, are 62% and 77%, respectively, of the MarM247 base metals properties. In contrast, the tensile and yield strengths of the Ni–Cr–Zr joints, produced at 1238°C/4 h, are 61% and 69%, respectively, of the MarM247 base metals properties. This clearly shows that as the time at temperature is increased for the Ni–Cr–Zr joints, the tensile and yield strengths increased. Also as seen in Table 5, the ductility of the Ni–Cr–Hf joints, produced at 1238°C/12 h, followed by a 1232°C/4 h SHT, and then followed by a 1080°C/4 h HIP, are 76% of the MarM247 base metals ductility. In contrast, the ductility of the Ni–Cr–Hf joints, produced at 1238°C/4 h, are 41% of the base metals ductility. This clearly showed that as the time at temperature is increased for the Ni–Cr–Hf joints, so too did the ductility. Similarly as seen in Table 5, the ductility of the Ni–Cr–Zr joints, produced at 1238°C/12 h, followed by a 1232°C/4 h SHT, and then followed by a 1080°C/4 h HIP, are 92% of the MarM247 base metals ductility. In contrast, the ductility of the Ni–Cr–Zr joints, produced at 1238°C/4 h, are 83% of the base metals ductility. This clearly showed that as the time of temperature is increased for the Ni–Cr–Zr joints, the ductility levels increased.

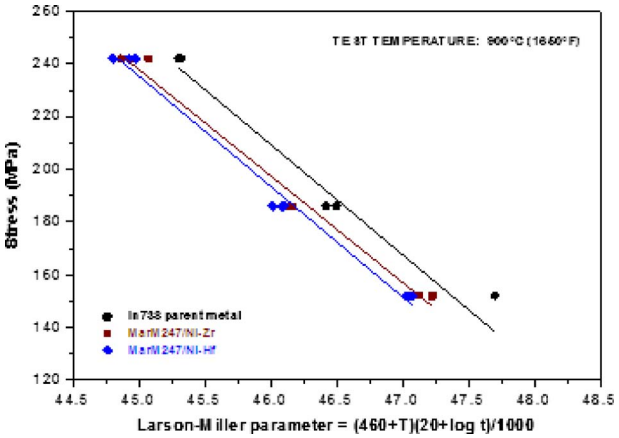

Fig. 19 Larson–Miller plot of the two brazed joints (produced at 1238°C for 12 h followed by a 1232°C for 4 h solution heat treatment) tested at 900°C at various stresses/loads

5.2 Stress Rupture Results and Discussion. Brazed joints for stress rupture testing were produced at 1238°C for 12 h followed by a 1232°C for 4 h SHT.

As can be seen in Fig. 19, the stress rupture properties of the MarM247/Ni–Cr–Zr brazed joints at 900°C/242 MPa (1650°F/35 ksi) are 69.0% of the IN738 base metal properties; whereas the MarM247/Ni–Cr–Hf brazed joints are 64.0% of the IN738 base metal properties. Similarly at 900°C/186 MPa (1650°F/27 ksi) the MarM247/Ni–Cr–Zr brazed joints are 71.0% of the IN738 base metal properties; whereas the MarM247/Ni–Cr–Hf brazed joints are 65.0% of the IN738 base metal properties. At 900°C/152 MPa (1650°F/22 ksi) the MarM247/Ni–Cr–Zr brazed joints are 77.0% of the IN738 base metal properties; whereas the MarM247/Ni–Cr–Hf brazed joints are 66.0% of the IN738 base metal properties. The Larson–Miller plot of Fig. 19, shows more precisely that the MarM247/Ni–Cr–Zr braze joints have superior stress rupture properties (7% superior) when compared with the MarM247/Ni–Cr–Hf brazed joints. In spite of the inferior stress rupture properties of the MarM247/Ni–Cr–-Hf brazed joints, when compared with the MarM247/Ni–Cr–Zr joints, the ductility of the former braze joints are superior to that of the latter brazed joints. The average elongation and RA of the MarM247/Ni–Cr–Hf brazed joints is 75% and 77% of the base metals values, respectively; whereas the average elongation and RA of the MarM247/Ni–Cr–Zr brazed joints is 63% and 68% of the base metals values, respectively. This implies that the Ni–Hf intermetallic phases are more ductile than the N–Zr intermetallic phases, and both intermetallic phases are far superior to the brittle boride phases by at least 100%, i.e., they are twice as ductile as the boride phases.

Typically, the average elongation values and RA values of brazed joints with B as a melting point depressant that form boride phases are 1–3% and 1–3%, respectively; whereas, the elongation and RA values of the Ni–Cr–Zr and Ni–Cr–Hf joints range from 4% to 6% and 5% to 9%, respectively.

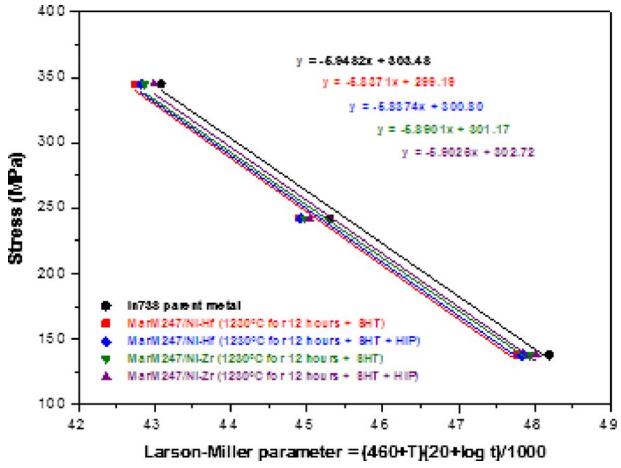

Fig. 20 Larson–Miller plot for the IN738 base metal and the MarM247/Ni–Cr–Hf and MarM247/Ni–Cr–Zr joints after brazing for 12 h at 1238°C, followed by solution heat treatment (SHT) of 1232°C/4 h of 1232 and a HIP cycle

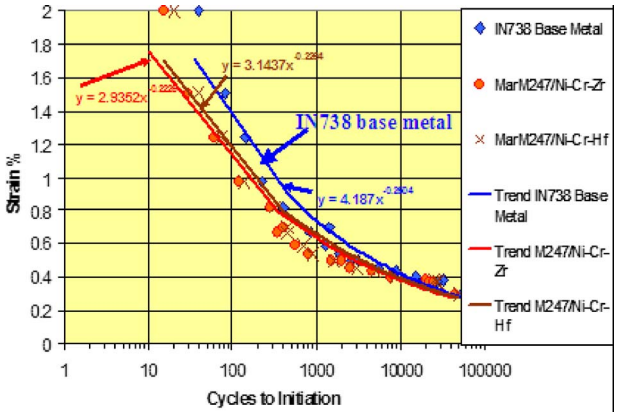

Fig. 21 LCF Properties at 870°C of IN738 Base Metal versus the MarM247/Ni–Cr–Zr & MarM247/Ni–Cr–Hf wide gap brazed joints

The results shown in Fig. 20 illustrate that the HIP cycle resulted in an improvement in the stress rupture properties of both the Ni–Cr–Hf and Ni–Cr–Zr braze joints. The best stress rupture properties were obtained in the MarM247/Ni–Cr–Zr joints after brazing at 1238°C/12 h, followed by a solution heat treatment at 1232°C/4 h, and a HIP cycle at 1080°C for 4 h at 175MPa. Depending on the test temperature, these joints displayed stress rupture lives between 74% and 89% of that of the base metal. Since the joints were tested in the partially solutioned heat treated condition, the stress rupture properties are expected to improve further once the full aging heat treatment is employed.

Although linear regression methods revealed very little statistically relevant difference between the lines representing the braze joints in Fig. 20, the Larson–Miller plot can be used to rank the braze joints in order of descending stress rupture properties.

- MarM247/Ni–Cr–Zr joint brazed at 1230°C for 12 h, followed by solution heat treatment, and a HIP cycle.
- MarM247/Ni–Cr–Zr joint brazed at 1230°C for 12 h and followed by solution heat treatment.
- MarM247/Ni–Cr–Hf joint brazed at 1230°C for 12 h and followed by solution heat treatment and a HIP cycle.
- MarM247/Ni–Cr–Hf joint brazed at 1230°C for 12 h and followed by solution heat treatment.

It is important to note that the improved stress rupture properties displayed by the braze joints after the HIP cycle cannot be attributed only to the closure of micropores in the microstructure. The higher stress rupture properties are most likely due to the precipitation of fine γ' precipitates within the MarM247 powder particles during the HIP cycle. Although equivalent base metal stress properties were not achieved, excellent joint ductility was obtained. For example, during testing at an applied stress level of 138 MPa at 980°C, both the Ni–Cr–Zr and Ni–Cr–Hf braze joints displayed ductility values in the region of 87% of that of the base metal. This implies that the presence of the Ni_7Hf_2 or Ni_5Zr intermetallic compound within the braze alloy did not embrittle the joints to the same extent as the boride phases observed in Ni–B braze alloys. In boride-containing braze joints, the ductility values rarely exceed 30% of the ductility of the base metal in the case of wide joint gaps.

These stress rupture samples were not age heat treated at 1121°C for 2 h+843°C for 24 h, typical of what would occur, when a component is repaired. Nevertheless, this data still provide a relevant comparison between the Ni–Cr–Zr and Ni–Cr–Hf braze joints. Since the material is tested in the partially solutioned heat treated condition, one would expect the material to be annealed (soft) and exhibit enhanced ductility, and reduced stress rupture strength. Therefore, the absolute stress rupture properties of the joints are expected to improve after the age heat treatment but the ductility marginally decreased. In this partially solution heat treated condition, the stress rupture properties of the Ni–Cr–Hf and Ni–Cr–Zr joints are between 65% and 75% of the IN738 base metals properties. Typically, based on past experience, with brazed joints using a Ni–B system, the age heat treatment will produce an increase in stress rupture properties of 15–20%. Therefore, if these samples were age heat treated, the properties of the Ni–Cr–Zr and Ni–Cr–Hf joints are expected to increase to 80–90% of the base metals properties.

5.3 Low Cycle Fatigue Results and Discussion. As seen in Fig. 21, the IN738 base metal has the highest LCF properties, followed by the MarM247/Ni–Cr–Hf and MarM247/Ni–Cr–Zr brazed joints. The LCF graph in Fig. 21 can be divided into three regions.

(a) Below 0.4% strain, the Ni–Cr–Zr braze has 85% of the base metals life and the Ni–Cr–Hf braze has 96% of the base metals life. Typically different repair authorities have different acceptance and rejection criteria, but it is safe to say that if a brazed joint has 70% or more of the base metals LCF life, then the braze filler can be utilized for production braze repairs of cracks on stationary nozzle segments. Unfortunately, only a few cracks do occur in regions of a nozzle where the strain is less than 0.4%.

(b) Between 0.4% and 0.8% strain, the region of strain were most cracks occur on a nozzle segment, it can be seen that the Ni–Cr–Zr braze has 70% of the base metals life and the Ni–Cr–Hf braze has 74% of the base metals life.

(c) Between 0.8% and 2% strain, where typically one or two cracks occur, none of the braze joints evaluated here have good LCF life. For a strain level of 1.5%, the Ni–Cr–Zr and Ni–Cr–Hf braze fail after 30 and 40 cycles, respectively. Comparing to the base metal failing after 80 cycles, it can be seen that none of the two braze filler metals come close to that of the base metals LCF properties at high strains.

6 Conclusions

A dense, low porosity wide gap brazed joint (processed at either 1238°C for 4 h or 1238°C for 12 h and/or followed by a 1232°C/4 h solution heat treatment or 1080°C for 4 h at 172.5

MPa HIP heat treatment) consisted of a two-phase microstructure, with coarse and fine grains. The γ dendrites/phases and Ni_5Zr or Ni_7Hf_2 phases existed intergranularly.

Increasing the brazing time from 4 h to 12 h at 1238°C, resulted in the reduction in thick continuous eutectic phases/films, and the reduction in the volume fraction of the γ dendrites/phases and Ni_5Zr or Ni_7Hf_2 phases. In fact in many areas only isolated and discrete γ dendrites/phases and Ni_5Zr or Ni_7Hf_2 phases existed.

At all tensile test temperatures, from 22°C to 980°C, the tensile and yield strength of the MarM247/Ni–Cr–Zr joints, produced either at 1238°C for 4 h or 12 h, are superior to those of the MarM247/Ni–Cr–Hf joints. The best tensile strength was achieved after brazing at 1238°C for 12 h, followed by a solution heat treatment of 1232°C for 4 h and a 1080°C for 4 h at 172.4 MPa HIP heat treatment.

The combination of brazing, solution heat treating, and HIP'ing resulted in the Ni–Cr–Zr joints having tensile and yield strengths as high as 98% and 100%, respectively, of the base metals strength. Similarly for the Ni–Cr–Hf joints, tensile and yield strengths were a high as 73% and 81%, respectively, of the base metals strength.

The combination of brazing, solution heat treating, and HIP'ing resulted in an improvement in the ductility of the braze joints, such that the MarM247/Ni–Cr–Hf and MarM247/Ni–Cr–Zr braze joints reached 78% and 92%, respectively, of the ductility of the base metal. Therefore, the presence of the Ni_7Hf_2 or Ni_5Zr intermetallic compound within the braze alloy does not embrittle the joints to the same extent as the boride phases observed in Ni–Cr–B braze alloys.

The best stress rupture properties were obtained for the MarM247/Ni–Cr–Zr joints and were on average 7% better than those of the MarM247/Ni–Cr–Hf joints. Depending on the test temperature, these joints displayed stress rupture properties between 74% and 89% of those of the base metal.

The MarM247/Ni–Cr–Zr and MarM247/Ni–Cr–Hf braze joints displayed LCF properties equivalent to those of the IN738 base metal at low strain rates (0.2–0.4% strain). At intermediate strain levels (0.4–0.8% strain), the Ni–Cr–Zr and Ni–Cr–Hf braze joints displayed 70% and 74%, respectively, of the LCF properties of the base metal. However, the LCF properties of the novel braze alloys at high strains were only 27% and 50%, respectively, of the base metal's LCF properties. The latter may appear to be a "poor" result but compared with the Ni–Cr–B braze alloys, these result of the novel braze alloys are an order of magnitude better.

Acknowledgment

Thanks to Professor Madeleine Du Toit, (my supervisor) for her thoughtful guidance throughout this thesis work.

References

[1] Lugscheider, E., and Kim, D. S., 1991, "New Low-Melting Nickel-Based High Temperature Brazing Alloys," Schweissen Schneiden, **43**(4), pp. 222–226.
[2] Lugscheider, E., and Partz, K. D., 1983, "High Temperature Brazing of Stainless Steel With Nickel-Base Filler Metals BNi-2, BNi-5 and BNi-7," Weld. J. Supplement (Miami, FL, U.S.), June, pp. 160s–164s.
[3] Sakamoto, A., Fujiwara, C., Hattori, T., and Sakai, S., 1989, "Optimizing Processing Variables in High Temperature Brazing, With Nickel-Based Filler Metals," Weld. J. (Miami, FL, U.S.), March, pp. 63–71.
[4] Draugelates, U., and Hartmann, K. H., 1978, "Behaviour of Brazed Nickel Alloy Under Cyclic and Thermal Load," Weld. J. Supplement (Miami, FL, U.S.), October, pp. 298s–302s.
[5] Tung, S. K., Lim, L. C., and Lai, M. O., 1996, "Solidification Phenomena in Nickel Base Brazes Containing Boron and Silicon," Scr. Mater., **34**(5), pp. 763–769.
[6] Gale, W. F., and Wallach, E. R., 1991, "Influence of Isothermal Solidification on Microstructural Development in Ni-Si-B Filler Metals," Mater. Sci. Technol., **7**, pp. 1143–1148.
[7] Wu, X. W., Chandel, R. S., Seow, H. P., and Li, H., 2001, "Wide Gap Brazing of Stainless Steel to Nickel Base Superalloy," J. Mater. Process. Technol., **113**, pp. 215–221.
[8] Tung, S. K., Lim, L. C., and Lai, M. O., 1995, "Microstructural Evolution and Control in BNi-4 Brazed Joints of Nickel 270," Scr. Metall. Mater., **33**(8), pp. 1253–1259.
[9] Leone, E. A., Rabinkin, A., and Sarna, B., 2006, "Microstructure of Thin Gauge Austenitic and Ferritic Stainless Steel Joints Brazed With Metglas Amorphous Foils," Weld. World, Sub COM 1A doc 1713-05/I-1147-041.
[10] Miyazawa, Y., and Ariga, T., 1993, "A Study of the Brazeability of Nickel Based Brazing Filler Metal Foils for Joining Nickel Base Metal to Mild Steel Base Metal," Weld. J. Supplement (Miami, FL, U.S.), July, pp. 294s–300s.
[11] Huang, X., Yandt, S., Nagy, D., and Yao, M., 2007, "Effect of Ruthenium, Rhenium and Yttria Additions on the Microstructure of Wide Gap Brazing on IN738," ASME Paper No. GT2007-27129.
[12] Fritsche, B., and Satir-Kolorz, A., 2000, "Repair Brazing of Ni-Base Turbine Blades," Weld. World, **44**(5), pp. 10–14.
[13] Van Esch, H., and Marijnissen, G., 1986, "Braze Repair Techniques," J. Turbomach., **9**, pp. 29–32.
[14] Demo, W. A., and Ferrigno, S. J., 1992, "Brazing Method Helps Repair Aircraft Gas Turbine Nozzles," Advanced Materials and Processes, **41**, pp. 43–46.
[15] Ellison, K. A., Lowden, P., and Liburdi, J., 1992, "Powder Metallurgy Repair of Turbine Components," ASME Paper No. 92-GT-312.
[16] Schoonbaert, S., Huang, X., Yandt, S., and Au, P., 2007, "Brazing and Wide Gap Repair of X-40 Using Ni-Base Alloys," ASME Paper No. GT-2007-27340.
[17] O'Neil, W. M., and Kennedy, A., 2000, "Braze Repairing GT Components: Retrospective, Perspective and Prospective," *20th ASM Heat Treating Conference Proceedings*, Oct. 9–12, pp. 1040–1045.
[18] Juergon, W., and Malik, M. P., 1985, "Wide Gap Brazing in Maintenance of Turbine Guide Vanes," DVS-Ber., **98**, pp. 78–82.
[19] Elder, J. E., Thamburaj, R., and Patnaik, P. C., 1989, "Braze Repair of MA754 Aero Gas Turbine Engine Nozzles," presented at the Gas Turbine Expo Conference, Ontario, Canada, Jun. 4–8, Paper No. 89-GT-235.
[20] Lee, J. W., Murray, J. H., and Miller, J. A., 1985, "Development of a New Brazing Technique for Repair of Turbine Engine Components," Weld. J. (Miami, FL, U.S.), **64**, pp. 18–21.
[21] Nash, P., and Nash, A., 1991, *ASM Handbook, Vol. 3: Alloy Phase Diagrams*, p. 241.
[22] Nash, P., and Jayanth, C., 1991, *ASM Handbook, Vol. 3: Alloy Phase Diagrams*, p. 322.
[23] Miglietti, W., Kearney, J., and Pabon, L., 2001, "Liquid Phase Diffusion Bond Repair of Siemens V84.2, Row 2 Vanes and Alstom Tornado, 2nd Stage Stator Segments,"ASME Paper No. 2001-GT-0510.
[24] Miglietti, W., Curtis, R., Hall, B., and Lazarin, C., 2000, "Liquid Phase Diffusion Bond Repair of Westinghouse, W501F, Row 3 Vanes," ASME Paper No. 2000-GT-0339.
[25] Miglietti, W., 2001, "Wide Gap Diffusion Braze Repair of Ni-Based Industrial Turbine Vanes," presented at the LOT Conference, Aachen, Germany.
[26] Huang, X., and Nagy, D., 2008, "Wide Gap Braze Repair Using Vertically Laminated Repair Scheme," ASME Paper No. GT2008-50046.
[27] Laux, B., Piegert, S., and Rosler, J., 2008, "Fast Epitaxial High Temperature Brazing of Single Crystalline Nickel Based Superalloys," ASME Paper No. GT2008-50055.